

Supporting Information

Hydrogen-Bonded Supercoil Self-Assembly from Achiral Molecular Components with Light-Driven Supramolecular Chirality

Yangyang Wang,^{ab} Deyan Zhou,^a Haining Li,^a Ruiru Li,^a Yueyao Zhong,^{ab} Xuan
Sun,^{*a} and Xun Sun^b

[†]Key Laboratory for Colloid & Interface Chemistry, Shandong University, Education
Ministry, Jinan, 250100, P. R. China

[‡]State Key Lab of Crystal Materials, Shandong University, Jinan, 250100, P. R. China

E-mail: sunxuan@sdu.edu.cn

Content

1. Fluorescence spectra of the aggregate and azobenzene **A**.
2. FT-IR characterization of the intermolecular hydrogen-bonding formed between **A** and **M**.
3. TGA analysis of the complex **M•A₃**
4. Elemental analysis of the complex **M•A₃**
5. ¹H NMR analysis of the complex **M•A₃**

6. Wide-angle X-ray diffraction (WAXD) patterns of the supercoils
7. UV-vis and CD spectra of the supercoils upon 365 nm irradiation
8. TEM image of the supercoils after photoirradiation with 365 nm light.
9. Crystal structure of **M-BA**

1. Fluorescence spectra of the aggregate and azobenzene **A**

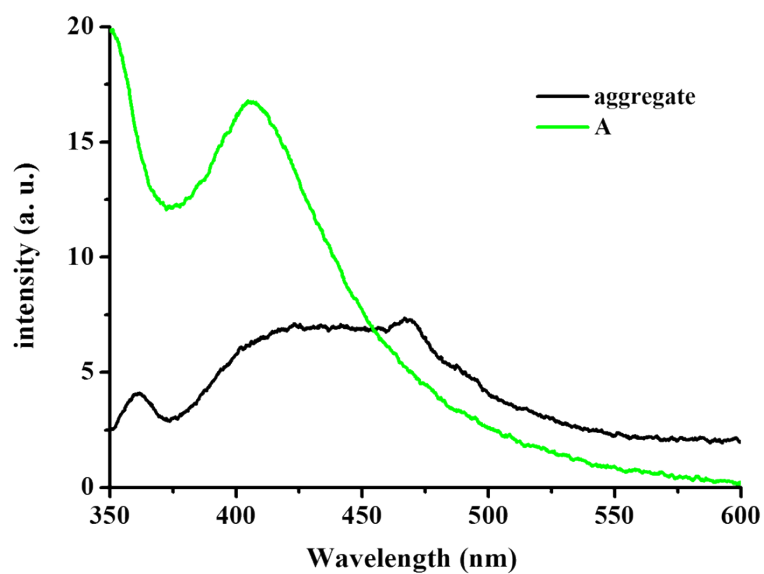


Figure S1. Fluorescence spectra of the self-assembled suspensions in water and the highly dispersed molecule **A** in THF at $c = 2.5 \times 10^{-5} \text{ mol L}^{-1}$, respectively.

2. FT-IR characterization of the intermolecular hydrogen-bonding formed between **A** and **M**.

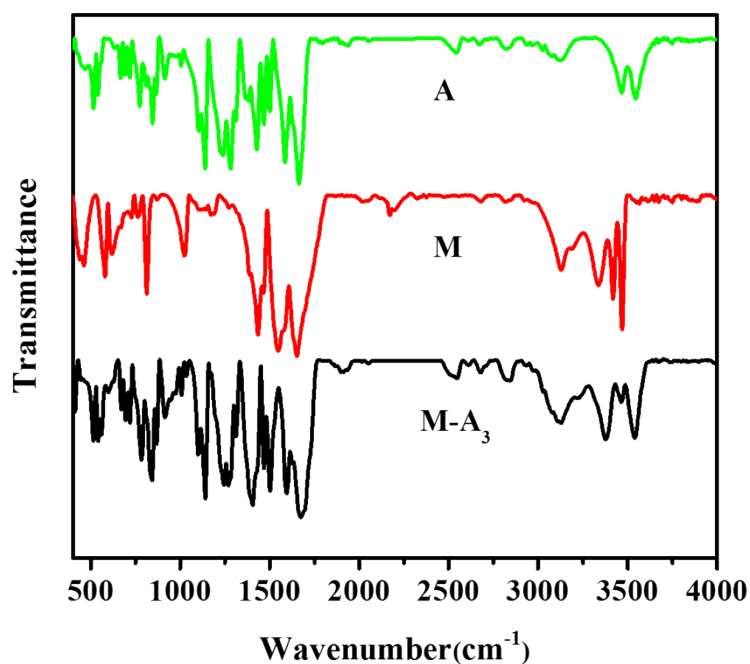


Figure S2. Comparison of the IR spectra of **A**, **M** and **M-A₃** complex at room temperature.

3. TGA analysis of the complex **M•A₃**

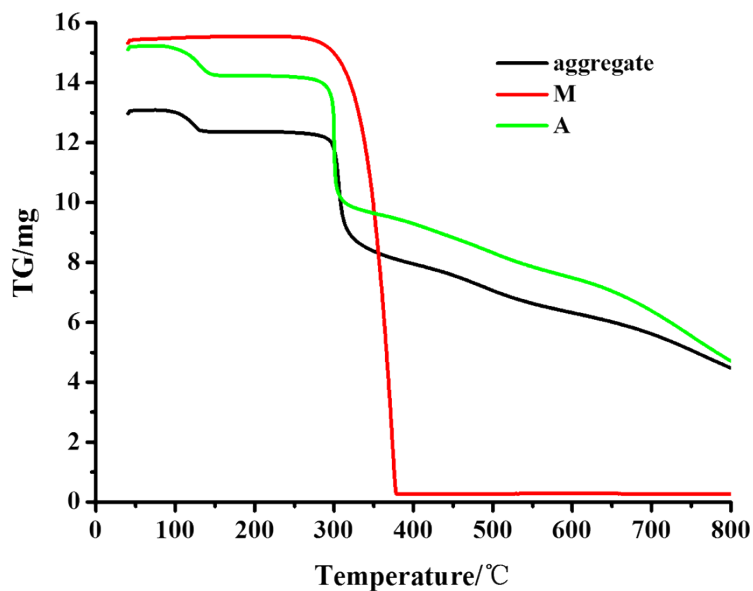


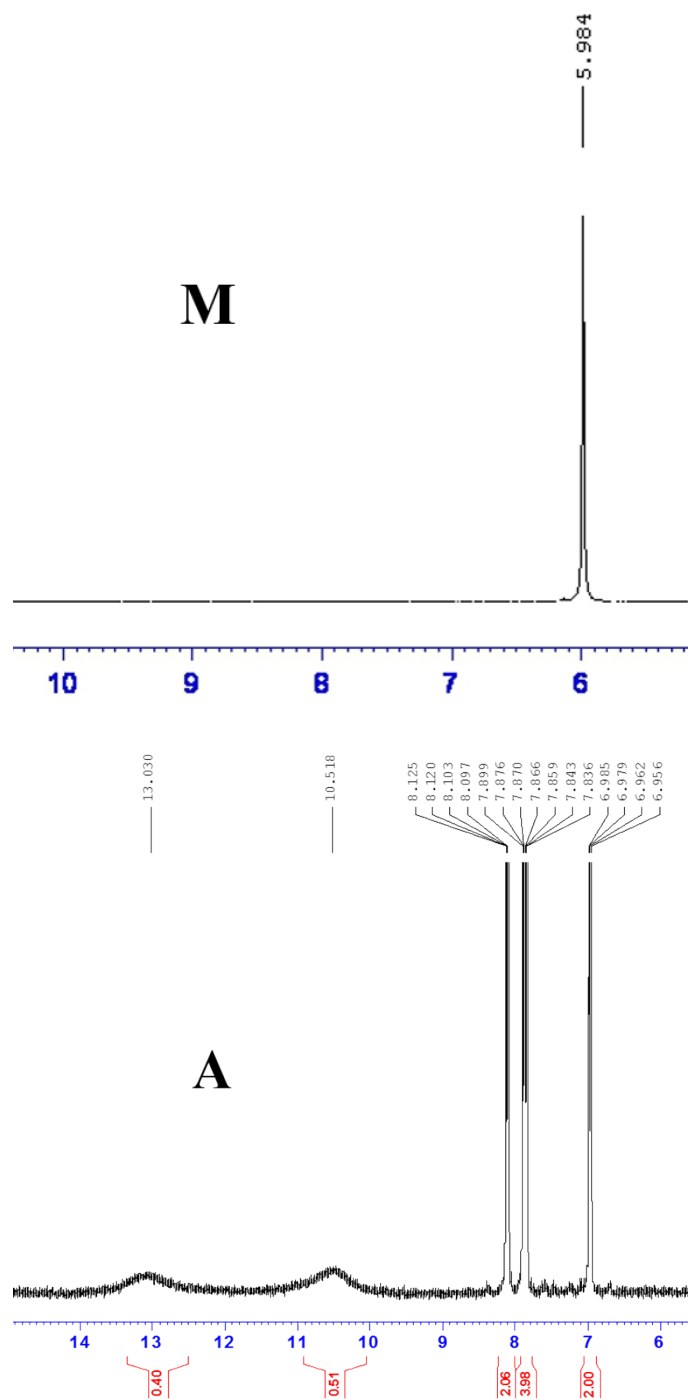
Figure S3. Thermalgravimetric analysis of **A**, **M**, and **M•A₃** complex in 3:1 ratio.

4. Elemental analysis of the complex $M \cdot A_3$

Table S1. Elemental analysis of the complex $M \cdot A_3$

Element	N	C	H	O
Percentage%	17.06	53.85	4.722	24.368

5. 1H NMR analysis of the complex $M \cdot A_3$



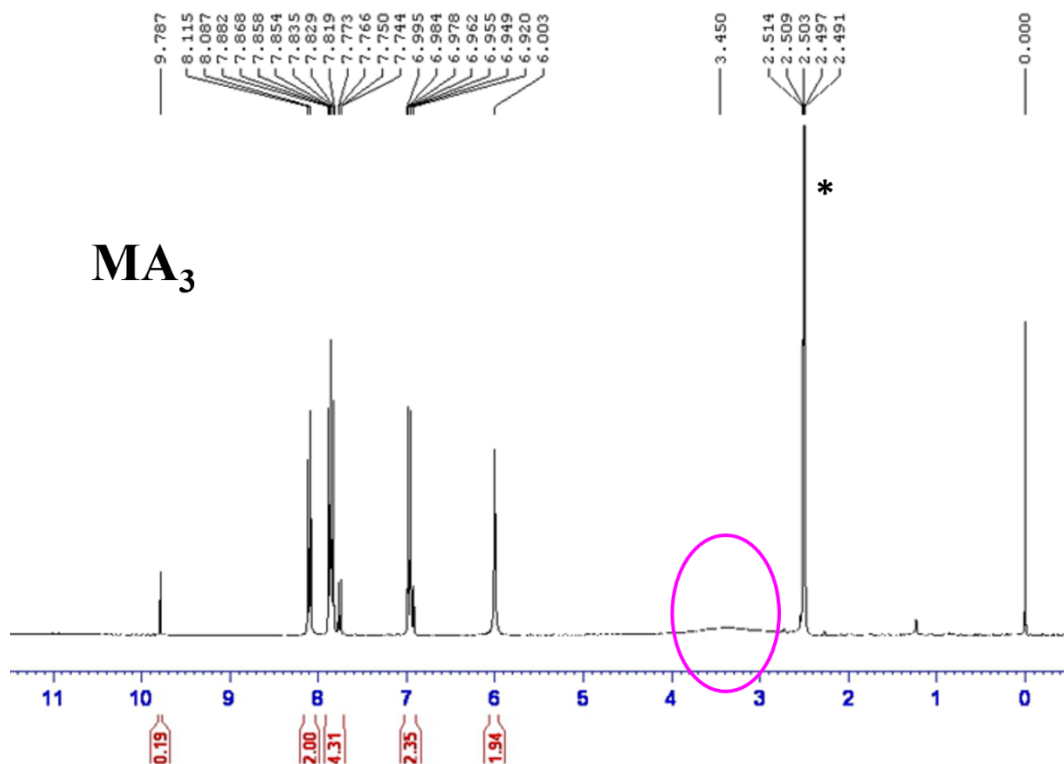


Figure S4. ^1H NMR spectrum of **M**, **A** and **M•A₃** using the residual solvent resonance of DMSO (denoted as *) at 2.505 ppm relative to SiO_2 as an internal reference.

6. Wide-angle X-ray diffraction (WAXD) patterns of the supercoils

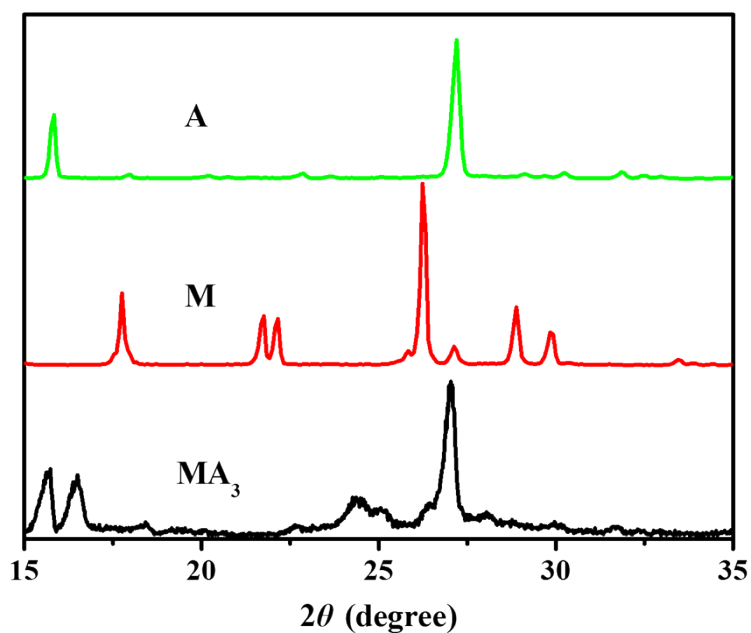


Figure S5. WAXD patterns of the solid **A**, solid **M**, and the supercoils formed from **M•A₃**

7. UV-vis and CD spectra of the supercoils upon 365 nm irradiation

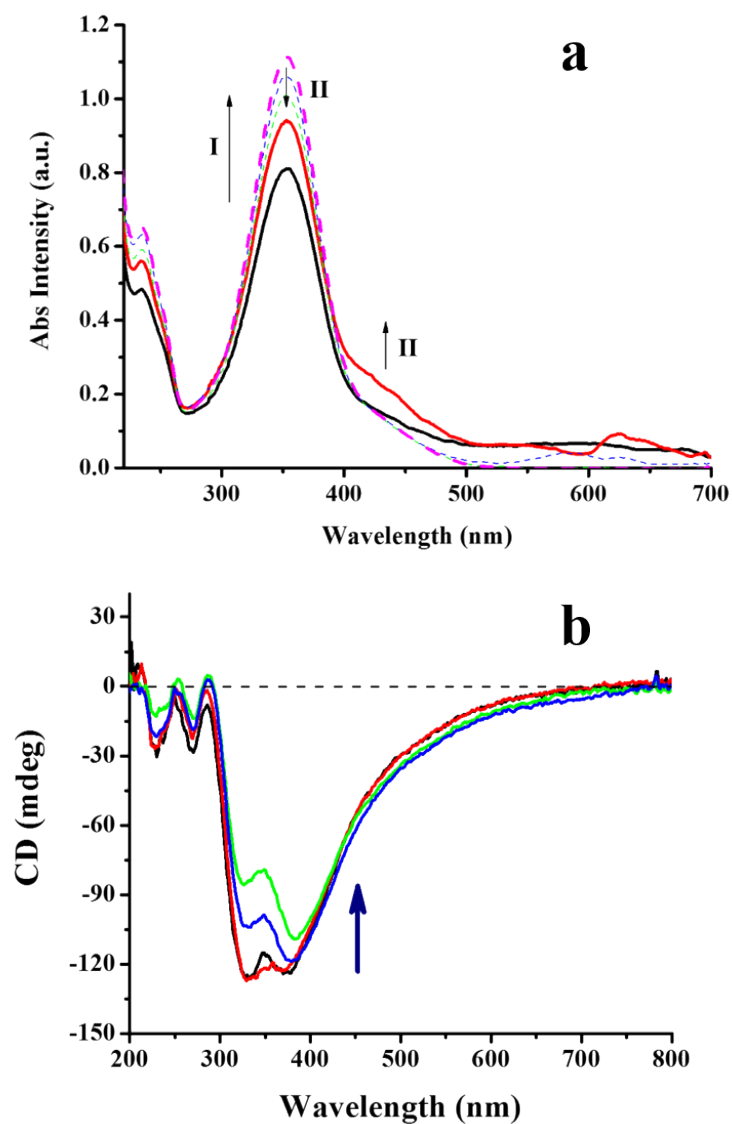


Figure S6. (a) UV-vis spectra and (b) CD spectra indicate the structure changes of the supercoils upon 365 nm irradiation. Two stages of changes in the absorption spectra are observed as indicated by the arrows.

8. TEM image of the supercoils after photoirradiation with 365 nm light.

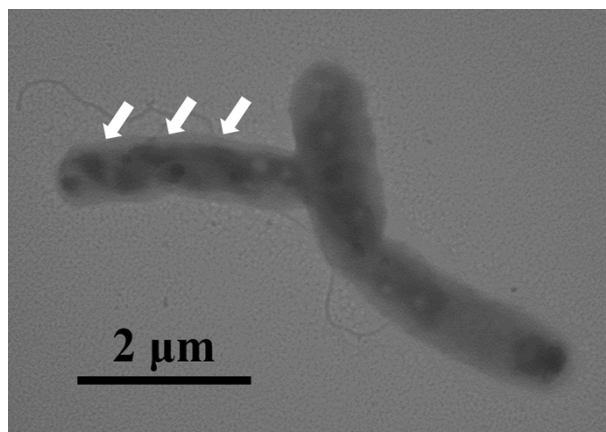


Figure S7. TEM image of the supercoils after photoirradiation with 365 nm light. The arrows indicate the remaining helical sense of the supercoils.

9. Crystal structure of **M-BA**

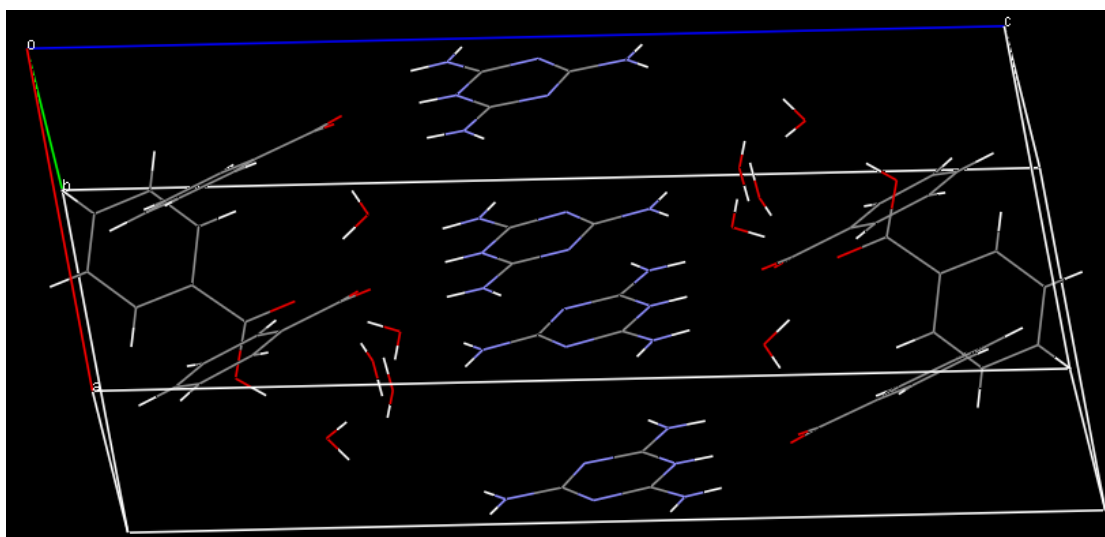


Figure S8. Side view of the hydrogen-bonding network within the crystal of **M-BA**. Protons on the $-\text{COOH}$ of **BA** are transferred onto the N atom of the triazine, and the $-\text{C}-\text{O}$ bonds of the benzoic acid units are identical. Highly ordered water channels inside the nanorods through hydrogen bonding, and the direction of the channels is parallel to the direction of the crystal growth.